Comparative infrared study of optimally doped and underdoped $La_{2-x}Sr_xCuO_4$ single crystals

2008 J. Phys.: Condens. Matter 20 075230

(http://iopscience.iop.org/0953-8984/20/7/075230)

IOP PUBLISHING JOURNAL OF PHYSICS: CONDENSED MATTER

J. Phys.: Condens. Matter **20** (2008) 075230 (9pp) doi:10.1088/0953-8984/20/7/075230

Comparative infrared study of optimally doped and underdoped $La_{2-x}Sr_xCuO_4$ single crystals

B Pignon[1], G Gruener[1], V Ta Phuoc[1], F Gervais[1], C Marin[2] and L Ammor[1]

[1] Laboratoire d'Electrodynamique des Matériaux Avancés, UMR 6157 CNRS-CEA, Université François Rabelais, Faculté des Sciences et Techniques, Parc de Grandmont, 37200 Tours, France

[2] Département de Recherche Fondamentale sur la Matière Condensée, Service de Physique Statistique, Magnétisme et Supraconductivité, CEA-Grenoble, 17 Rue des Martyrs, 28054 Grenoble Cedex 9, France

Received 6 June 2007, in final form 12 November 2007
Published 31 January 2008
Online at stacks.iop.org/JPhysCM/20/075230

Abstract

The temperature dependence of the optical spectra of two $La_{2-x}Sr_xCuO_4$ single crystals was investigated for both in-plane and out-of-plane directions. For the underdoped ($x = 0.08$) single crystal, the in-plane optical conductivity that was analysed by a generalized Drude formalism shows a suppression of the scattering rate $1/\tau(\omega)$ and an increased effective mass m^* as the temperature decreases at low frequencies. Since this behaviour can be explained by the pseudogap effect, it is concluded that the pseudogap is not present at the optimal doping ($x = 0.15$). This result is confirmed by the c-axis optical conductivity, which decreases only for the underdoped single crystal. The absence of the pseudogap at the optimal composition is in accord with the quantum critical point model and it can explain the phase diagram of high-temperature superconductors.

(Some figures in this article are in colour only in the electronic version)

1. Introduction

Beyond the superconducting state, the diagram of temperature–carrier concentration (T, p) has many phases whose interactions have been intensively investigated. The existence of a pseudogap state in the normal state of underdoped high-temperature superconductors (HTSCs) is now widely accepted [1]. This corresponds to anomalous physical properties below a temperature T^*, the so-called pseudogap temperature, higher than the superconducting transition temperature T_C. These anomalous characteristics are observed by magnetic [2], transport [3, 4], thermodynamic [5], neutron diffraction [6] and optical measurements [7] in various cuprates. To understand the superconducting mechanism, it will be necessary to elucidate the origin of the pseudogap state and its interaction with the superconducting state. The pseudogap is defined as a decrease in the density of states at the Fermi level. Two major scenarios are proposed to explain the phase diagram of HTSCs. In the first one, the pseudogap phase represents a precursor to the superconducting phase with preformed pairs without phase coherence below T^*. The coherence phase would be acquired in the superconducting state below T_C due to the Fermi liquid behaviour expected in the overdoped regime [8]. One of the major corresponding models is the resonating valence bond (RVB) model based on spin/charge separations [9]. In this model, the pseudogap phase is present in the slightly overdoped regime. In the second scenario, the pseudogap would end up in the superconducting phase in a quantum critical point (QCP) [10]. According to this idea, different phases compete with one another, and the pseudogap can be associated with either an ordered [11] or a disordered phase [12]. The order parameter associated with these competing phases may involve charge and spin density waves [13], charge currents flowing around the CuO_2 square lattice [14], or orbital circulating currents [10]. According to Lavrov *et al*, in La-doped Bi-2201 single crystals, two distinct mechanisms are responsible for the pseudogap. The first one is insensitive to the magnetic field in the underdoped region and must be related to

magnetic correlations or stripes. The second one is sensitive only in the superconducting samples and is suppressed when the magnetic field is applied along the c-axis [15].

The temperature T^* at which the pseudogap effects start to be seen can be determined by several experimental techniques. However, different crossover temperatures T^* have been used in the literature and the observed pseudogap in the density of states is very sensitive to the specific physical property used to define it. For example, the angle resolved photoemission data obtained by Nagano [16], probing the charge excitations in $YBa_2Cu_3O_{6+\delta}$, led to a gap two times larger than the gap observed by nuclear magnetic resonance and inelastic neutron experiments [17]. Although many works seem to indicate that the pseudogap continues in the slightly overdoped regime, its presence for the optimal composition is still debatable. In fact, experimental results seem to depend on the system studied and the technique employed. In the Bi-2212 system, Miyakawa *et al* observed a pseudogap phase in slightly overdoped compounds by tunnelling spectroscopy [18]; Ozyuzer *et al* reported its absence in heavily overdoped samples [19] and Santander-Syro *et al* showed no pseudogap signature in the normal state conductivity of underdoped and overdoped thin films [20]. Moreover, in the LSCO compounds, Häfliger *et al* observed the pseudogap in a heavily doped $La_{1.71}Sr_{0.25}Ho_{0.04}CuO_4$ sample by neutron experiments but recent results of Fauque *et al* suggested the absence of the pseudogap for the optimally doped composition [6]. The work of Boebinger *et al* on the resistivity of LSCO single crystals with a pulsed magnetic field supported the existence of a QCP [21]. In fact, the existence or absence of the pseudogap state at the optimal doping, like the presence of a QCP, is still debated.

Optical spectroscopy is a fundamental technique for probing the electronic state of a superconductor. Indications of normal state gap-like anomalies are also observed in infrared optical measurements in-plane and out-of-plane. In c-axis infrared conductivity, the pseudogap feature can be observed in the form of a gap-like region of depressed conductivity at low frequency. As the temperature is lowered below T^*, Homes *et al* observed a decrease in the optical conductivity, at low frequencies, with an amplitude evolution that is comparable to the NMR Knight shift of Cu(2) in $YBa_2Cu_3O_{6.70}$ [22]. One should also note that the conductivity in the c-axis pseudogap region is flat and frequency independent. A pseudogap in the c-axis conductivity has also been seen in $YBa_2Cu_4O_8$ compounds [23], in underdoped $YBa_2Cu_3O_7$ [24] and in underdoped $Pb_2Sr_2(Y/Ca)Cu_3O_8$ [25]. In the single-layered $La_{2-x}Sr_xCuO_4$, evidence of the presence of a pseudogap is controversial. In fact, the c-axis conductivity depression does not show the strong gap signature seen in the two-plane YBaCuO systems [26–28]. Basov *et al* found the conductivity to be depressed in the normal state for slightly underdoped crystal $x = 0.15$ over a very large frequency range of 1000 cm^{-1} [26]. Recently, Uchida *et al* [27] and Startseva *et al* [28] found reduced normal state conductivity at frequencies below ~500–600 cm^{-1} in underdoped LSCO $x = 0.12$ and 0.13, respectively. Generally, the reported studies on the c-axis conductivity showed that the depression is not as prominent as that found in two-layer compounds [26, 28]. Clearer evidence of a pseudogap in the underdoped LSCO system came from the scattering rate and conductivity along CuO_2 in the far-infrared region, as generally reported.

The in-plane optical conductivity spectra can be described by a peak at $\omega = 0$ and a long tail at higher frequencies up to around 7000 cm^{-1} [24]. Two principal approaches are commonly used, called 'one-component' and 'two-component', to describe this behaviour. In the first, both the peak and the tail are due to the same carriers with a strong scattering rate $1/\tau(\omega)$ and effective mass $m^*\omega$-dependent. The scattering rate increases rapidly with the frequency, consequently a large $1/\tau$ is responsible for the long tail at high frequencies and a small $1/\tau$ is responsible for the sharp peak at very low frequencies. This empirical approach is based on the generalized Drude formalism where the conductivity is described by the relation [7]

$$\tilde{\sigma} = \frac{\omega_P^2}{4\pi} \frac{1}{1/\tau(\omega, T) - i\omega m^*/m(\omega, T)} \tag{1.1}$$

where ω_P is the plasma frequency of the corresponding carriers.

In the 'two-component' approach, two different contributions are assumed: the Drude response of free carriers and a second band of 'mid-infrared' carriers. In this picture, the optical conductivity can be described by a dielectric function model, which is based on Lorentzian oscillators. For example, the in-plane optical conductivity can be reproduced from the complex dielectric function [29]:

$$\tilde{\varepsilon}(\omega) = \varepsilon_\infty - \frac{\Omega_{PD}^2}{\omega(\omega + i\gamma_D)} + \sum \frac{\Delta\varepsilon_j \Omega_j^2}{(\Omega_j^2 - \omega^2 - i\gamma_j\omega)}. \tag{1.2}$$

The optical conductivity is calculated using the following relation:

$$\tilde{\sigma}(\omega) = i\varepsilon_V\omega(1 - \tilde{\varepsilon}(\omega)). \tag{1.3}$$

In equation (1.2), the first term ε_∞ refers to the constant dielectric value at high frequencies. The second term is the Drude expression where Ω_{PD} is the plasma frequency of the free carriers, smaller than ω_P, and γ_D is the damping. The last term is the Lorentzian oscillator sum which corresponds to optical phonons, the mid-IR band or charge transfer excitations. Ω_j, γ_j and $\Delta\varepsilon_j$ correspond, respectively, to the frequency, the damping and the strength of the oscillator. ε_V is the dielectric vacuum constant. The optical conductivity along the c-axis can also be described by this dielectric function model. In this case, the Drude term is generally omitted due to the semiconducting behaviour along this axis.

The in-plane optical data have mainly been discussed in the literature within the framework of the extended Drude model. In this case, the scattering rate $1/\tau$ and the mass enhancement are interpreted to be strongly frequency dependent. It is generally suggested, especially for underdoped samples, that a suppression of the optical scattering rate $1/\tau$, as determined from the extended Drude analysis of reflectance spectra, below a typical constant energy scale $\omega \sim 700$ cm^{-1}, irrespective of temperature and doping, is the infrared signature

of the pseudogap state. In fact, the term signature is used because there is no relation between the value of the scattering rate and the density of states at the Fermi level. To explain the difference between the *ab*-planes and the *c*-axis, recent work of Santander *et al* suggested that the optical conductivity is sensitive to the Fermi velocity of the quasiparticles $\mathbf{v}_F$ [20]. The latter will be more important in the nodal direction (π, π) where the pseudogap is closed. Consequently, the scattering rate $1/\tau$ will be smaller in this direction, because a reduced number of states leads to an increased life time and decreased scattering. Because the pseudogap is opened in the antinodal direction $(0, \pi)$ the optical conductivity of the *ab*-planes will not be sensitive to the pseudogap opening. For this reason, in order to observe the pseudogap phase, in the conductive planes we had to show a $1/\tau$ depression at low frequencies. Similarly, the optical conductivity of the *c*-axis will be more sensitive to antinodal quasiparticles, so that the pseudogap is observed directly. In the past, Puchkov *et al*, Basov *et al* and Wang *et al* [7, 30, 31] referred to such a gap-like suppression of $1/\tau$ to the pseudogap in the *ab*-plane optical response in a series of underdoped compounds (Y123; Y124; Bi2212, Y-doped Bi2212 and Tl2201). In contrast, at the optimal doping and in the strongly overdoped regime this gap-like depression is not seen.

For LSCO, various in-plane differences have been reported [28, 32–36]. Some of these reported spectra that show rich features in the far-infrared (FIR) region are ascribed either to the excitation of *ab*-plane TO-phonons [28] or the excitations related to the polarons [33–35]. In general, the difficulty in studying the optical data obtained on LSCO system is related to the difficulty in obtaining a pure in-plane spectrum. This problem originates from the large anisotropy in the electronic system of LSCO where only a small amount of the *c*-axis component causes a serious effect on in-plane-spectrum [37]. Another problem is a structural phase transition temperature from the low-temperature orthorhombic phase to the high-temperature tetragonal phase. It was been shown that this transition temperature decreases with increasing doping [38]. Both these phenomena complicate the analysis of the optical spectra of this system, and the presence of the pseudogap in this material is somewhat controversial.

Here we will focus on the behaviour of $1/\tau$ pertaining to the debate about the presence of a pseudogap in the case of LSCO compounds. Indications of normal state, gap-like anomalies in underdoped LSCO were observed in the *ab*-plane optical conductivity measurements by Startseva *et al* [28]. They showed that a pseudogap could be seen below a temperature T^* which is well above room temperature in several underdoped ($x = 0.13$ and 0.14) compounds. The gap is defined as the region of depressed scattering below the high-frequency linear behaviour. One should note that in the case of the two-plane materials, $1/\tau$ is temperature independent in the pseudogap temperature region, i.e. $T < T^*$. Recently, infrared reflectivity measurements on overdoped $La_{2-x}Sr_xCuO_4$, with $x = 0.184$ and 0.22, suggest that the pseudogap persists into the overdoped state [39]. Furthermore, while the high-frequency part of $1/\tau$ is linear and temperature independent in the underdoped regime, it becomes temperature dependent as doping is increased above optimal levels. A similar observation was obtained on an overdoped epitaxial $La_{2-x}Sr_xCuO_4$ ($x = 0.17$) thin film [32]. Those authors found a strongly temperature-dependent scattering rate even at low temperatures. It can be concluded that the opening of the pseudogap and the temperature-independent high-frequency $1/\tau$ both add up to a very peculiar state of electron dynamics in underdoped high-T_c superconducting materials. The scattering depression below 700 cm^{-1} in both underdoped ($x = 0.1$) and optimally doped ($x = 0.15$) has also been reported by Calvani *et al* [35]. However, the $1/\tau$ increases for $\omega < 100$ cm^{-1}, in contradiction to the usual interpretation of the pseudogap in terms of suppression of the scattering channel for the carriers. An unphysical sign change for the effective mass m^* at energies lower than 100 cm^{-1} is also observed in this study. It is argued that, by using a multi-component analysis, these observations support the existence of other charges that can be excited at low energy, in addition to the Drude quasiparticles.

In this paper we will study two $La_{2-x}Sr_xCuO_4$ single crystals, one underdoped ($x = 0.08$) and another optimally doped one ($x = 0.15$), by infrared measurements. These will be analysed in the conductive *ab*-planes and in the semiconducting *c*-axis, from 4 to 300 K, in order to study the pseudogap phase, and particularly at the optimal doping.

2. Experiment and characterization

The single crystals of $La_{2-x}Sr_xCuO_4$ have a cylindrical shape with a diameter of 6 mm and a height of 3 mm. They were grown by the travelling solvent floating zone technique [40]. X-ray and neutron diffraction have confirmed that the crystals are free from any foreign phases and their qualities are good with a mono-domain structure [28]. Moreover, their quality was confirmed by a scanning electron microscopy (SEM) study where no difference was observed with secondary and backscattered electrons. Many micrometric electron diffraction spectroscopy (EDS) analyses have been performed on the whole surface of the single crystals and show an average composition $La_{1.940(\pm0.007)}Sr_{0.072(\pm0.005)}Cu_{0.98(\pm0.01)}O_{4+\delta}$ and $La_{1.867(\pm0.012)}Sr_{0.151(\pm0.007)}Cu_{0.981(\pm0.008)}O_{4+\delta}$ for the $x = 0.08$ and 0.15 single crystals, respectively. As indicated, the dispersion is very low between the measurements showing the good homogeneity of the samples.

As suggested by Tajima *et al* [35], the cutting and polishing steps of the samples were performed very carefully in order to avoid the mixing of the conductive *ab*-planes with the semiconductive *c*-axis [41]. The crystals were aligned using Laue diffraction and polished to be parallel to the CuO_2 planes. Measurements on both *ab*-planes and the *c*-axis were done. The critical temperature, which was determined by both magnetization and resistivity measurements, was found to be 28 K for the underdoped composition $x = 0.08$ and 38 K for $x = 0.15$, the optimally doped composition. The results of the resistivity and magnetization measurements on the same single crystals used in the optical measurements are shown in figure 1. These measurements were obtained with a Quantum Design PPMS-372 system.

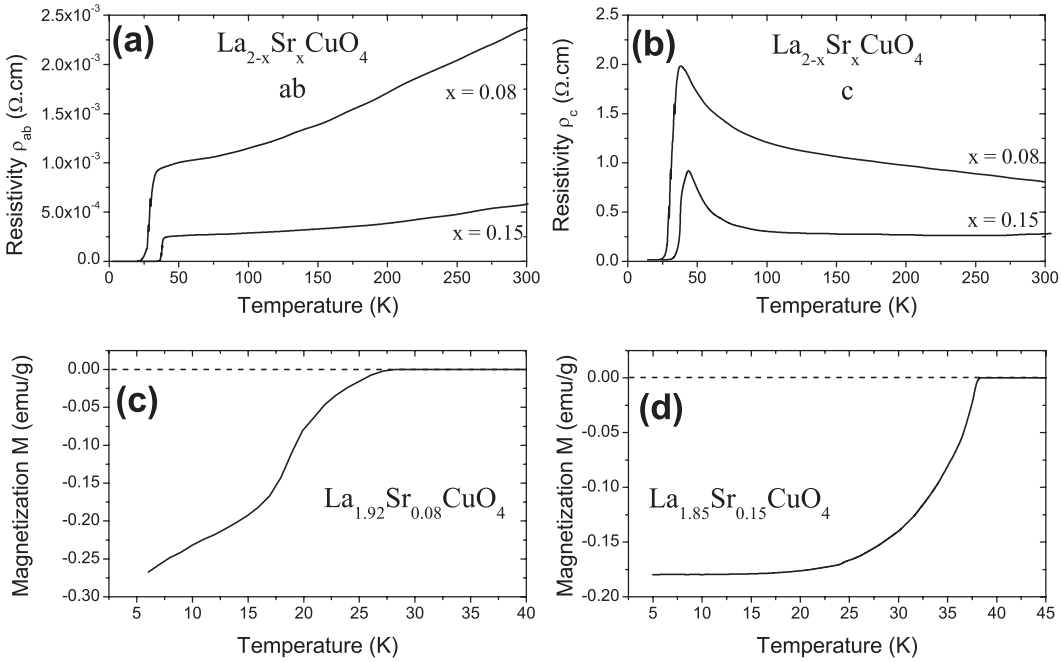

Figure 1. In-plane (a) and out-of-plane (b) resistivity of the two single crystals. Their magnetization curves are shown in (c) and (d). The superconducting transition temperatures T_C are 28 and 38 K for $La_{1.92}Sr_{0.08}CuO_4$ and $La_{1,85}Sr_{0.15}CuO_4$, respectively.

The reflectivity spectra were taken by a Bruker IFS 66v interferometer from 60 to 8000 cm^{-1} for the underdoped sample and 12 000 cm^{-1} for the optimally doped one. A He gas-flow cryostat was used to stabilize the temperature between 4 and 300 K. Polarizers were used to separate the contribution of CuO_2 planes from the *c*-axis optical response. An evaporated Au film was used as the reference mirror. The coincidence of spectra in each of the overlap frequency ranges does not exceed 0.5%. The different fits and calculus of the curves were performed by using FOCUS software [42].

3. Results and discussions

3.1. The pseudogap and the ab-plane scattering rate

The reflectivity curves $R_{ab}(\omega, T)$ of the *ab*-planes of the two single crystals are shown in figure 2. The reflectivity is temperature dependent, dropping as temperature increases. For both samples, the low-ω reflectance $R_{ab}(\omega)$ displays a metallic T dependence, which is in agreement with the dc transport measurements. However, as we can see from figure 2, there is a more pronounced temperature dependence of reflectivity of the underdoped sample in comparison to the optimally doped one. The plasma edges are observed at around 7000 and 7500 cm^{-1} for the two single crystals of $x = 0.08$ and 0.15, respectively. The plasma edge is more pronounced in the case of the optimally doped crystal due to its more significant carrier content. The results of Startseva *et al* on underdoped $La_{2-x}Sr_xCuO_4$ with $x = 0.13$ and 0.14 showed a plasma edge around 7800 cm^{-1} [28]. According to a group theory with D_{4h}^{17} symmetry, $\Gamma_{opt} = 3A_{2u} + 4E_u + B_{2u} + 2A_{1g} + 2E_g$. For $E \parallel c$, only the (A_{2u}) infrared modes are active. In the planes, there are four infrared-active modes: Eu(1) at around 680 cm^{-1},

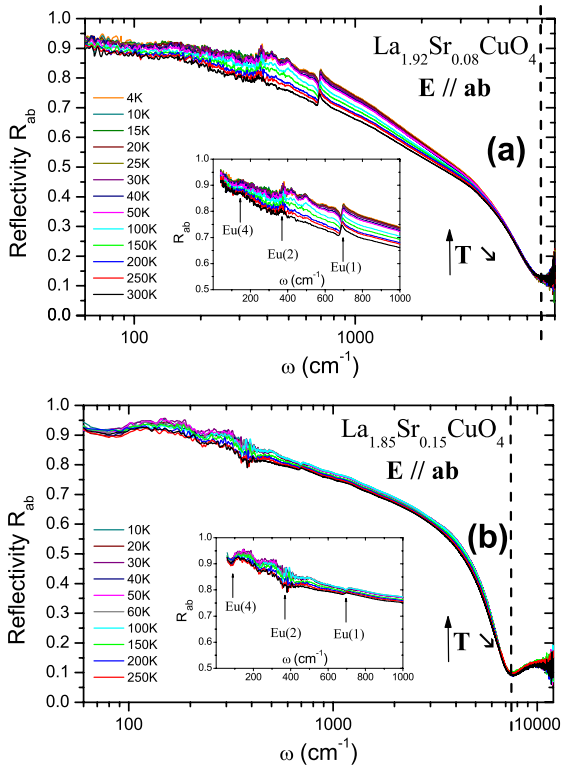

Figure 2. In-plane reflectivity of $La_{1.92}Sr_{0.08}CuO_4$ (a) and $La_{1.85}Sr_{0.15}CuO_4$ (b) with a semilog representation for the frequencies. The insets show the values at low frequencies relating to the optical phonons. Dashed lines represent the plasma edge.

Eu(2) at around 360 cm^{-1}, Eu(3) at around 220 cm^{-1} and Eu(4) at around 140 cm^{-1} [43]. Of all the observed peaks, only Eu(3) is identified as not having already been mentioned

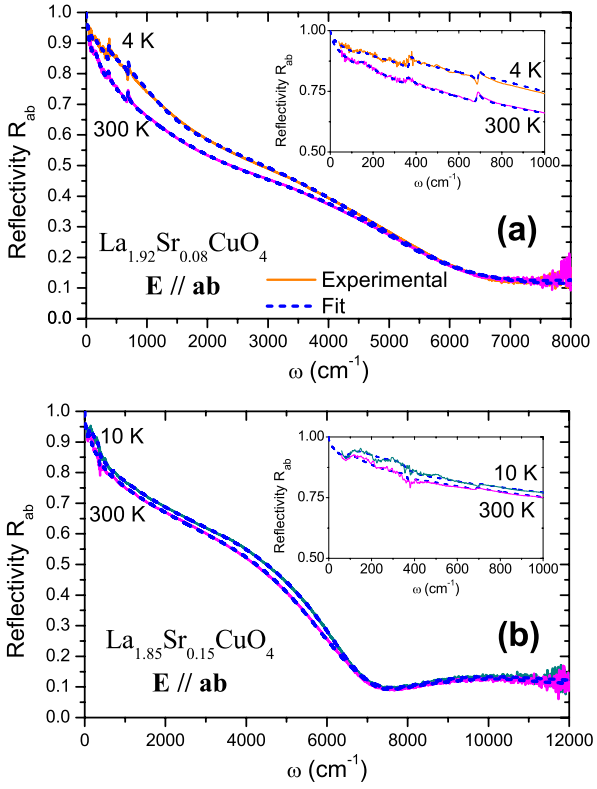

Figure 3. In-plane reflectivity curves of $La_{1.92}Sr_{0.08}CuO_4$ (a) and $La_{1.85}Sr_{0.15}CuO_4$ (b) with the corresponding fits calculated from equation (1.2). The values at low frequencies are shown in the inset. For the sake of clarity, only the extreme temperatures are shown.

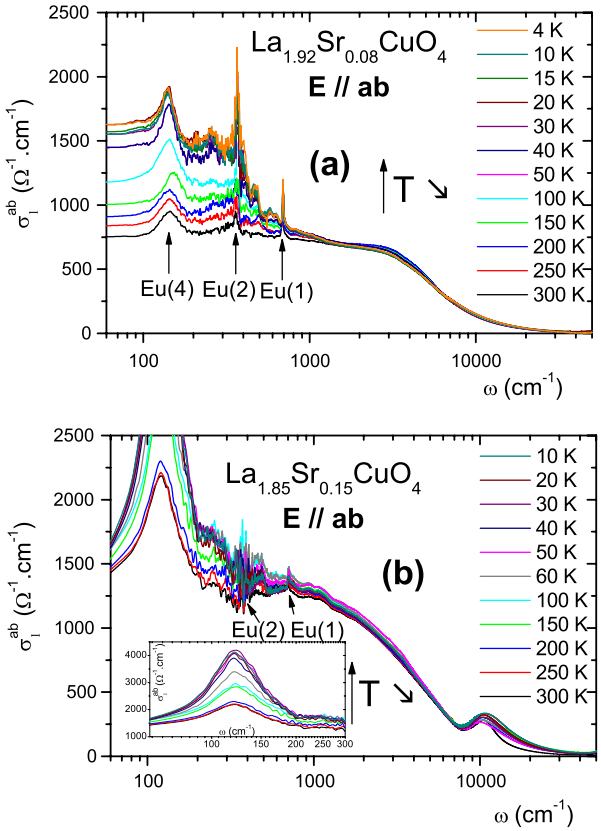

Figure 4. Real part of the in-plane optical conductivity of $La_{1.92}Sr_{0.08}CuO_4$ (a) and $La_{1.85}Sr_{0.15}CuO_4$ (b) calculated from Kramers–Kronig transformations. Optical phonons are mentioned. The question mark mentioned for the Eu(4) phonon indicates that the corresponding peak probably has a different origin.

by other authors [44, 45]. This can be understood by the weakness of the corresponding oscillator. Our reflectivity data agree well with reported results on single crystals of the same composition [28, 36]. This confirms that our samples are not miscut and there is no polarizer leakage.

The complex optical conductivity $\tilde{\sigma}(\omega)$ was obtained by Kramers–Kronig transformations of the reflectivity data. Since this analysis requires knowledge of the reflectivity values at all frequencies, extrapolations must be used at low and high frequencies. To determine the corresponding data, we have fitted the reflectivity curves by using the relation (1.2) and a two-component approach. In the latter, the three phonons and a mid-IR band have been introduced as Lorentzian oscillators. Some authors identified the mid-IR band in polaron terms [46]. For the optimally doped single crystals, one oscillator was added between 8000 and 12 000 cm^{-1} attributed as charge transfer excitation [47]. Examples of the fits are presented in figure 3. The real parts of the optical conductivity calculated for the two single crystals are shown in figure 4. As the temperature decreases, the conductivity increases below 1500 cm^{-1}. For the underdoped sample, a decrease of spectral weight at low frequencies, which can be attributed to the pseudogap behaviour, can be seen clearly [28]. The optical phonons are indexed. An atypical peak evolution is observed for the optimally doped single crystal around 110 cm^{-1}. This frequency is lower than the value predicted and calculated for the lowest infrared-active phonon of LSCO (132 cm^{-1}) [44]. This peak is the consequence of the observed dip in the reflectivity curve (figure 2) at the same frequency. Such a peak is often observed in $HgBa_2Ca_2Cu_3O_{8+\delta}$ and is expected more in optimally doped samples than in underdoped ones [48, 49]. A large peak centred at $\omega \sim 110$ cm^{-1} in our study was also seen in many HTSCs which are intrinsically disordered including $Tl_2Ba_2CuO_{6+\delta}$ [50] and $YBa2(Cu_{1-x}Zn_x)_4O_8$ [51]. In the LSCO system this peak was observed in the overdoped LSCO single crystals [38], but was absent in the LSCO thin films [32]. Many authors have assigned the peaks at low frequencies to an unambiguous manifestation of stripes or carrier localization [33–35]. Further investigations should be performed in order to clarify their origin. It will be particularly interesting to study the anisotropy in the electronic response of the *ab*-planes to support the stripes notion as recently mentioned by Padilla *et al* [52].

Another picture of the pseudogap state can be seen from the effective scattering rate, $1/\tau(\omega, T)$, calculated from the conductivity using equation (1.1) which is shown in figure 6. To calculate it, we have used the fits of the optical conductivity where we have subtracted contributions from phonons and charge transfer excitation (figure 5) to conserve only the electronic and mid-IR contributions. The subtraction was performed by using the FOCUS software [53]. The scattering rate $1/\tau(\omega, T)$ and the effective mass were determined by

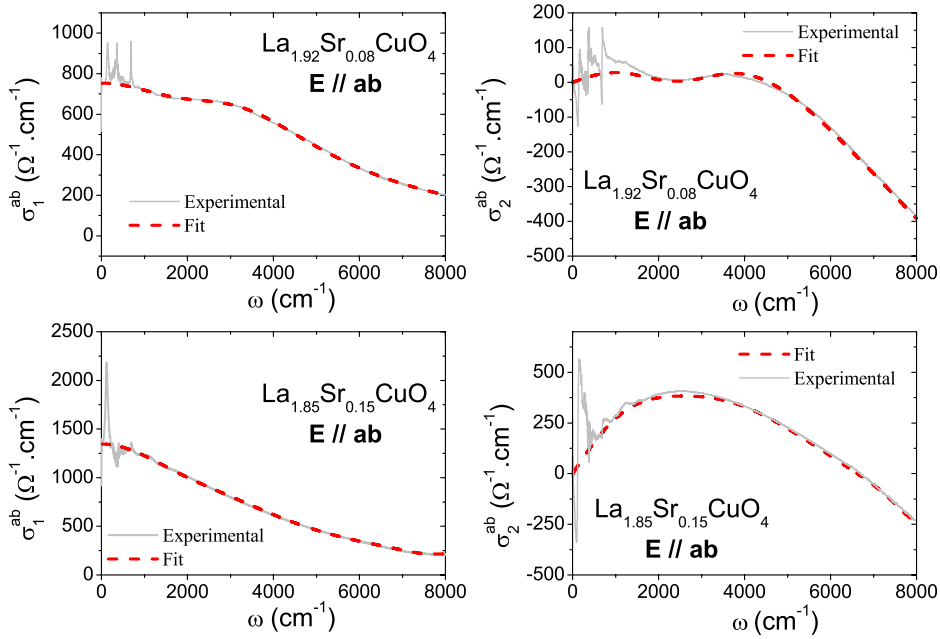

Figure 5. Real part σ_1^{ab} and imaginary part σ_2^{ab} of the optical conductivity of $La_{1.92}Sr_{0.08}CuO_4$ and $La_{1.85}Sr_{0.15}CuO_4$ at $T = 300$ K. The corresponding fits, where the optical phonons were subtracted, are shown.

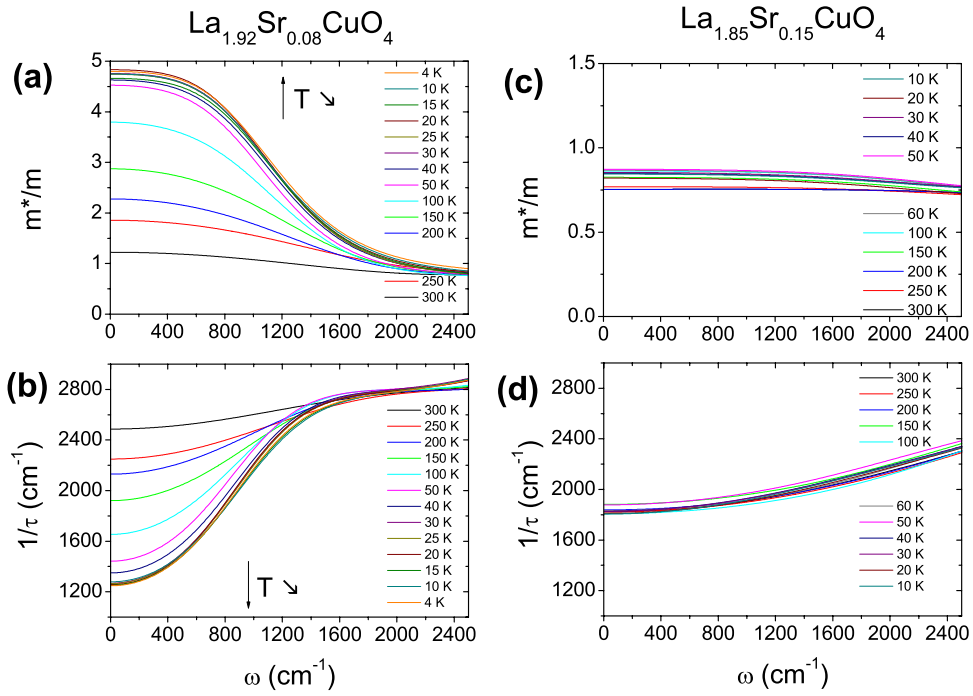

Figure 6. Effective mass m^*/m and scattering rate $1\tau(\omega, T)$ of $La_{1.92}Sr_{0.08}CuO_4$ ((a), (b)) and $La_{1.85}Sr_{0.15}CuO_4$ ((c), (d)).

using the following relations:

$$\frac{1}{\tau(\omega, T)} = \frac{\omega_P^2}{4\pi} \mathrm{Re}\left(\frac{1}{\tilde{\sigma}(\omega, T)}\right) \tag{3.1}$$

$$\frac{m^*(\omega, T)}{m_e} = \frac{1}{\omega}\frac{\omega_P^2}{4\pi} \mathrm{Im}\left(\frac{1}{\tilde{\sigma}(\omega, T)}\right) \tag{3.2}$$

that were deduced from equation (1.1).

The ω_P plasma frequency was obtained from the integral:

$$\omega_P^2 = \frac{2m_e}{\pi e^2}\int_0^{\omega_0} \sigma_1(\omega)\, \mathrm{d}\omega \tag{3.3}$$

where m_e and e are the electron mass and charge, respectively. We have chosen the cut-off frequency $\omega_0 = 8000$ cm^{-1} so that the integral range includes the reflectance plasma edge and excludes the charge transfer excitation energy

($>10\,000$ cm^{-1}) [54]. We have not considered the plasma frequency Ω_{PD} obtained from the fits (equations (1.1), (1.2)) because these were calculated with the hypothesis of the Drude model with free carriers.

In figure 6 we show the spectra of the scattering rate and the effective mass for the underdoped and the optimally doped samples. As observed in figure 6, for the underdoped sample, in the high-frequency region, the scattering rate varies linearly with frequency while in the low-frequency region there is a clear suppression of $1/\tau$ below this linear behaviour. For the underdoped sample, the suppression of $1/\tau$ can be seen not only at low temperature but at also at temperature much higher than T_C. A weak suppression is even seen at room temperature. This result suggests the presence of a pseudogap phase only in the underdoped region for the LSCO system. We also note that the low-frequency depression in $1/\tau$ at $T < T^*$ is accompanied by an increase in the effective mass at low frequencies and temperatures, as already reported by Startseva *et al* [28]. The pseudogap opening temperature T^* is defined as the temperature where the decrease at low temperatures appears. According to our data, T^* is larger than 300 K for the $La_{1.92}Sr_{0.08}CuO_4$ single crystal. We can see that, for the optimally doped sample, $1/\tau$ shows an upward curvature. The effective mass $m^*(\omega)$ does not show any temperature dependence and remains largely flat over the whole frequency region shown. This is in contrast with the $1/\tau$ and m^* behaviour in the underdoped sample. The $1/\tau$ and m^* behaviour of the optimally doped sample is very similar to what is observed in the overdoped $Tl_2Ba_2CuO_{6+\delta}$ single crystals [7, 55].

Let compare our results with data of Startseva *et al* on the underdoped ($x = 0.13$ and 0.14) [28] and the overdoped ($x = 0.184$ and 0.22) $La_{2-x}Sr_xCuO_4$ single crystals [39]. Firstly, the infrared reflectivity measurements of Startseva *et al* suggest that the pseudogap persists into the overdoped state. This is in sharp contrast to our results and the previous Raman scattering experiments on an overdoped $La_{1.78}Sr_{0.22}CuO_4$ single crystal which shows no sign of a pseudogap [56]. The other observation that can be made from the work of Startseva *et al* is that a sharp peak around 500 cm^{-1} and a broad peak below 200 cm^{-1} found in $1/\tau$ spectra can be considered as the admixture effect. As mentioned by Tajima *et al*, these peaks could originate from a c-axis component which seriously influences the $1/\tau$ behaviour [37]. In our investigation, we do not observe such peaks in scattering rate spectra. In conclusion, the absence of the pseudogap in the optimal composition agrees with the QCP scenario. Actually, its presence is not predicted at the optimal doping.

3.2. The pseudogap in the c-axis conductivity

The pseudogap feature can also be observed in the c-axis IR conductivity in the form of a gap-like region of depressed conductivity at low frequency. The spectral weight decrease is observed at low frequencies and it can be understood as a consequence of the decrease of density of states at the Fermi level [22]. Consequently, the pseudogap effect can be directly observed in the optical conductivity curves.

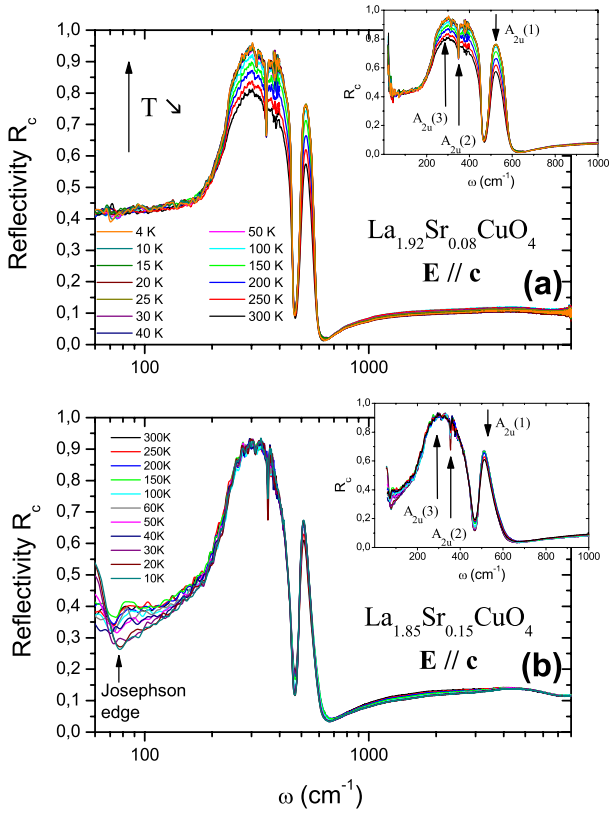

Figure 7. c-axis reflectivity of $La_{1.92}Sr_{0.08}CuO_4$ (a) and $La_{1.85}Sr_{0.15}CuO_4$ (b) with a semilog representation for the frequencies. The insets show the values at low frequencies to indicate the optical phonons. The Josephson plasma edge of $La_{1.85}Sr_{0.15}CuO_4$ is indicated by an arrow.

In figure 7 we present the c-axis reflectivity data at temperatures below and above T_C for the two samples. At low frequencies, there is no coherent Drude peak, in agreement with the semiconductive behaviour of the c-axis. These curves are essentially dominated by optical phonons. The temperature dependence of reflectivity is more pronounced in the underdoped single crystal. For the optimally doped one, a Josephson plasma edge can be observed, at temperatures $T < T_C$ around 70 cm^{-1}. This is explained by the coherence of the superconducting carriers. In fact, the c-axis conductivity is too low so that the tunnelling of Cooper pairs between the planes (Josephson current) can be observed. Recent results of Kim *et al* on $La_{2-x}Sr_xCuO_4$ with $x = 0.07$ and 0.09 showed a Josephson plasma edge around 20 cm^{-1} [57]. This value is not observed for our underdoped sample because it is not within the range of our measurement systems.

Similar to the procedure used for the conductive planes, the reflectivity was fitted by using the dielectric model. For the underdoped single crystal, the Drude term was omitted and three optical phonons were used as Lorentzian oscillators: $A_{2u}(1)$, $A_{2u}(2)$ and $A_{2u}(3)$ at around 490, 350 and 220 cm^{-1}, respectively, in agreement with previous works [43, 44]. In the case of the optimally doped single crystal, the Drude term was not neglected due to the fact that the carrier concentration is higher. To consider the observed Josephson plasma edge, as proposed by Dordevic *et al* [58], a Drude term without

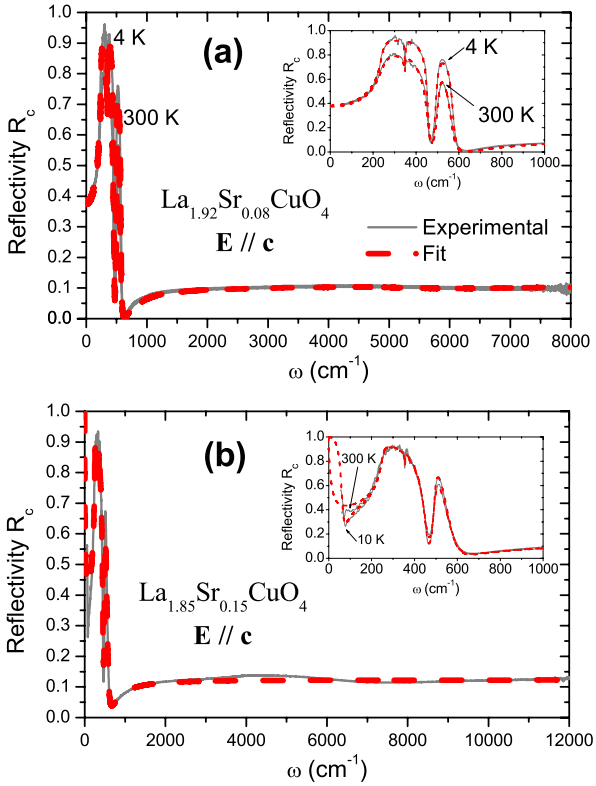

Figure 8. c-axis reflectivity curves of $La_{1.92}Sr_{0.08}CuO_4$ (a) and $La_{1.85}Sr_{0.15}CuO_4$ (b) with the corresponding fits calculated from equation (1.2). The values at low frequencies are represented in the inset. For the sake of clarity, only the extreme temperatures are shown.

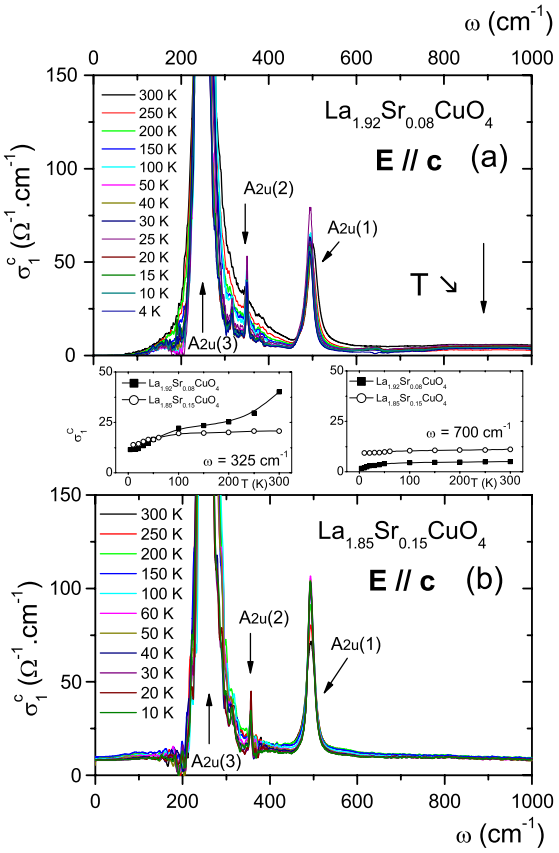

Figure 9. Real part of the optical conductivity of $La_{1.92}Sr_{0.08}CuO_4$ (a) and $La_{1.85}Sr_{0.15}CuO_4$ (b) calculated from Kramers–Kronig transformations. Optical phonons are mentioned. In the insets are represented the c-axis conductivity temperature dependence at $\omega = 325$ and 700 cm^{-1}.

damping was added. Figure 8 shows the fits for the two extreme temperatures measured.

As in the conductive planes, the real part of the c-axis optical conductivity was calculated by Kramers–Kronig transformations of the data shown in figure 8. The corresponding conductivity, shown in figure 9, is low and is dominated by optical phonons. It should be noted that the temperature dependence of the optical conductivity is more pronounced for the underdoped single crystal compared to the optimally doped one. This is in accordance with a very weak T dependence of ρ_c for $x = 0.15$ (see figure 1). In the very low-frequency ($\omega < 100$ cm^{-1}) range, the conductivity $\sigma(\omega)$ in the normal state is nearly ω independent and is higher for the optimally doped sample due to a larger carrier content. On the other hand it appears, as seen in figure 8 for $x = 0.08$, that the electronic contribution is extremely low to follow the T dependence of $\sigma(\omega)$ for this sample, in the low-frequency region. Similar behaviour has been reported for underdoped $La_{2-x}Sr_xCuO_4$ ($x = 0.1$) [27, 59]. Nevertheless, the data show a low-frequency depression of the c-axis conductivity only in the underdoped sample between 200 and 500 cm^{-1} as shown in the inset of figure 9. The c-axis conductivity at 325 cm^{-1} is depressed below 300 K and could be a signature of the pseudogap due to the decrease in the density of states at the Fermi level. This behaviour is identical to the reported c-axis conductivity measured at 450 cm^{-1} of an underdoped $La_{1.87}Sr_{0.13}CuO_4$ single crystal [28]. Based on this analysis, it can be deduced that the pseudogap state in the c-axis direction is opened below 300 K. This result confirms the existence of the pseudogap in only the underdoped sample. Nevertheless, we conclude that our findings in the direction perpendicular to the CuO_2 planes showed that the depression of the c-axis conductivity is not as prominent as that found in the high-temperature superconductors with two CuO_2 layers like the $YBa_2Cu_3O_{7-\delta}$ compound [22]. Clearer evidence of a pseudogap came from the scattering rate and conductivity along CuO_2 in the far-infrared region.

4. Conclusion

Two single crystals of $La_{2-x}Sr_xCuO_4$ were studied by infrared measurements where $x = 0.08$ and 0.15. The measurements were performed in the conductive ab-planes and the semiconductive c-axis. In the case of the ab-planes, the real part of the optical conductivity of the underdoped ($x = 0.08$) single crystal clearly shows a pseudogap behaviour with a decrease of the scattering rate and an increase of the effective mass at low frequencies. These results are not observed in the optimally doped single crystals ($x = 0.15$). The c-axis optical conductivity decreases with temperature at low frequency for the underdoped one. This result is interpreted again by the

pseudogap effect. Because this decrease is not observed for the optimal composition, it is concluded that the pseudogap is only present in the underdoped composition. In the QCP scenario, the pseudogap phase is not predicted at the optimal doping in agreement with the results obtained in this work.

References

[1] Timusk T and Statt B 1999 *Rep. Prog. Phys.* **62** 61
[2] Alloul H, Ohno T and Mendels P 1989 *Phys. Rev.* B **63** 1700
[3] Ito T, Takenaka K and Uchida S 1993 *Phys. Rev. Lett.* **70** 3995
[4] Watanabe T, Fujii T and Matsuda A 1997 *Phys. Rev. Lett.* **79** 2113
[5] Loram J W, Mirza K A, Wade J M, Cooper J R and Liang W Y 1997 *Physica* C **235** 134
[6] Fauque B, Sidis Y, Hinkov V, Pailhes S, Lin C T, Chaud X and Bourges P 2006 *Phys. Rev. Lett.* **96** 197001
[7] Puchkov A V, Basov D N and Timusk T 1996 *J. Phys.: Condens. Matter* **8** 10049
[8] Emery V J and Kivelson S A 1995 *Nature* **374** 434
[9] Anderson P W *The Theory of Superconductivity in the High T_c Cuprate Superconductors* (Princeton, NJ: Princeton University Press)
[10] Varma C M 2006 *Phys. Rev.* B **73** 155113
[11] Poilblanc D 2005 *Phys. Rev.* B **72** 060508
[12] Norman N and Pines D 2005 *Adv. Phys.* **54** 715
[13] Chen H D, Vafek O, Yazdani A and Zhang S C 2004 *Phys. Rev. Lett.* **93** 187002
[14] Chakravarty S, Laughlin R B, Morr D K and Nayak C 2001 *Phys. Rev.* B **63** 094503
[15] Lavrov A N, Ando Y and Ono S 2002 *Europhys. Lett.* **57** 267
[16] Nakano T, Naoki M, Migaku O and Masayuki I 1998 *J. Phys. Soc. Japan* **67** 2622
[17] Mihailovic D, Kabanov V V, Zagar K and Demsar J 1998 *Phys. Rev.* B **60** R6995
[18] Miyakawa N, Guptasarma P, Zasadzinski J F, Hinks D G and Gray K E 1998 *Phys. Rev. Lett.* **80** 157
[19] Ozyuzer L, Zasadzinski J F, Gray K E, Kendziora C and Miyakawa N 2002 *Europhys. Lett.* **58** 589
[20] Santander-Syro A F, Lobo R P S M, Bontemps N, Konstantinovic Z and Raffy H 2002 *Phys. Rev. Lett.* **88** 097005
[21] Boebinger G S, Ando Y, Passner A, Kimura T, Okuya M, Shimoyama J, Kishio K, Tamasaku K, Ichikawa N and Uchida S 1996 *Phys. Rev. Lett.* **77** 5417
[22] Homes C C, Timusk T, Liang R, Bonn R A and Hardy W N 1993 *Phys. Rev. Lett.* **71** 1645
[23] Basov D N, Timusk T, Dabrowski B and Jorgensen J D 1994 *Phys. Rev.* B **50** 3511
[24] Tajima S, Schutzman J and Miyamoto S 1995 *Solid State Commun.* **95** 759
[25] Reedyk M, Timusk T, Hsueh Y W, Statt B W, Xue J S and Greedan J E 1997 *Phys. Rev.* B **56** 9129
[26] Basov D N, Mook H A, Dabrowski B and Timusk T 1995 *Phys. Rev.* B **52** R13141
[27] Uchida S, Tamasaku K and Tajima S 1996 *Phys. Rev.* B **53** 14558
[28] Startseva T, Timusk T, Puchkov A V, Basov D N and Mook H A 1999 *Phys. Rev.* B **59** 7184
[29] Gervais F 2002 *Mater. Sci. Eng. Rep.* **39** 29
[30] Wang N L, Mcconnell A W, Clayman B P and Gu G D 1999 *Phys. Rev.* B **59** 576
[31] Basov D N, Liang R, Dabrowski B, Bonn D A, Hardy W N and Timusk T 1996 *Phys. Rev. Lett.* **77** 4090
[32] Gao F, Romero D B, Tanner D B, Talvacchio J and Forrester M G 1993 *Phys. Rev.* B **47** 1036
[33] Lucarelli A, Lupi S, Ortolani M, Calvani P, Maselli P, Capizzi M and Giura P 2003 *Phys. Rev. Lett.* **90** 037002
[34] Dumm M, Komiya S, Ando Y and Basov D N 2003 *Phys. Rev. Lett.* **91** 077004
[35] Calvani P, Ortolani M, Lucarelli A, Lupi S, Perla A, Maselli P and Fujita T 2002 *J. Supercond.* **15** 539
[36] Takenaka K, Shiozaki R, Okuyama S, Nohara J, Takayanagi Y and Sugai S 2002 *Phys. Rev.* B **65** 092405
[37] Tajima S, Fudamoto Y, Gorshunov B, Zelezny V and Uchida S 2007 *Phys. Rev.* B **71** 094508
[38] Weber W H, Peters C R and Logothetis E M 1989 *J. Opt. Soc. Am.* B **6** 455
[39] Startseva T, Timusk T, Okuya M, Kimura T and Kishio K 1999 *Physica* C **321** 135
[40] Marin C, Charvolin T, Braithwaite D and Calemczuk R 1999 *Physica* C **320** 197
[41] Tajima S, Uchida S, Van der Marel D and Basov D N 2003 *Phys. Rev. Lett.* **91** 129701
[42] Meneses D D S, Brun J F, Echegut P and Simon P 1994 *Appl. Spectrosc.* **58** 969
[43] Pintschovius L, Bassat J M, Odier P, Gervais F, Chevrier G, Reichardt W and Gompf F 1989 *Phys. Rev.* B **40** 2229
[44] Collins R T, Schlesinger Z, Chandrashekhar G V and Shafer M W 1989 *Phys. Rev.* B **39** 2251
[45] Gao F, Romero D B, Tanner D B, Talvacchio J and Forrester M G 1993 *Phys. Rev.* B **47** 1036
[46] Lupi S, Calvani P, Capizzi M, Maselli P, Sadowski W and Walker E 1992 *Phys. Rev.* B **45** 12470
[47] Calvani P, Capizzi M, Dore P, Lupi S, Maselli P, Paleologo G, Balestrino G, Marinelli L, Berger H, Roy P and Mathis Y L 1993 *Int. J. Infrared Millim. Waves* **14** 251
[48] Scuto A, Combescot R and Timusk T 1998 *Phys. Rev.* B **58** 11721
[49] McGuire J J, Windt M, Stratseva T and Timusk T 2000 *Phys. Rev.* B **62** 8711
[50] Puchkov A V and Timusk T 1995 *Phys. Rev.* B **51** 3312
[51] Basov D N, Dabrowski B and Timusk T 1998 *Phys. Rev. Lett.* **81** 213230
[52] Padilla W J, Dumm M, Komiya S, Ando Y and Basov D N 2005 *Phys. Rev.* B **72** 205101
[53] Meneses D D S *FOCUS* http://crmht.cnrs-orleans.fr/pot/software/focus.html
[54] Uchida S, Ido T, Takagi H, Arima T, Tokura Y and Tajima S 1991 *Phys. Rev.* B **43** 7942
[55] Ma Y C and Wang N L 2006 *Phys. Rev.* B **73** 144503
[56] Naeini J G, Chen X K, Hewit K C and Irwin J C 1998 *Phys. Rev.* B **57** R11077
[57] Kim Y H, Hor P H, Dong X L, Zhou G, Zhao Z X, Wu Z and Xiong J W 2005 *Phys. Rev.* B **71** 092508
[58] Dordevic S V, Komiya S, Ando Y and Basov D N 2003 *Phys. Rev. Lett.* **91** 167401
[59] Henn R, Wittlin A, Cadona M and Uchida S 1997 *Phys. Rev.* B **56** 6295